Refine Your Search Results

Micro and Nanostructures

Search

Sort By: Relevancy

Search Results

Found 35 results (Page 1)

Share These Results

Exact Match Found

MICRO AND NANOSTRUCTURES

Publisher: ACADEMIC PRESS LTD- ELSEVIER SCIENCE LTD , 24-28 OVAL RD, LONDON, ENGLAND, NW1 7DX

ISSN / eISSN: 2773-0123

Web of Science Core Collection: Science Citation Index Expanded

Additional *Web of Science* Indexes: Current Contents Physical, Chemical & Earth Sciences | Essential Science Indicators

Share This Journal

View profile page

** Requires free login.*

Other Possible Matches

Micro and Nanostructures

Latest issue

Volume 175

In progress

March 2023

About the journal

Formerly known as Superlattices and Microstructures;

Micro and Nanostructures is a journal disseminating the science and technology of micro-structures and nano-structures in materials and their devices, including individual and collective use of semiconductors, metals and insulators for the exploitation of their unique properties. The journal ...

View full aims & scope

3.3 weeks
Time to First Decision

5.3 weeks
Review Time

1 week
Publication Time

View all insights

Editor In Chief | View full Editorial Board

Micro and Nanostructures

Latest issue

Volume 175

In progress

March 2023

About the journal

Formerly known as Superlattices and Microstructures;

Micro and Nanostructures is a journal disseminating the science and technology of micro-structures and nano-structures in materials and their devices, including individual and collective use of semiconductors, metals and insulators for the exploitation of their unique properties. The journal ...

View full aims & scope

3.3 weeks
Time to First Decision

5.3 weeks
Review Time

1 week
Publication Time

View all insights

Editor In Chief | View full Editorial Board

Professor Deren Yang

Zhejiang University, China

Aims & Scope

Micro and Nanostructures is a journal disseminating the science and technology of micro-structures and nano-structures in materials and their devices, including individual and collective use of semiconductors, metals and insulators for the exploitation of their unique properties. The journal hosts papers dealing with fundamental and applied experimental research as well as theoretical studies. Fields of interest, including emerging ones, cover:

- Novel micro and nanostructures
- Nanomaterials (nanowires, nanodots, 2D materials) and devices
- Synthetic heterostructures
- Plasmonics
- Micro and nano-defects in materials (semiconductor, metal and insulators)
- Surfaces and interfaces of thin films

In addition to Research Papers, the journal aims at publishing Topical Reviews providing insights into rapidly evolving or more mature fields. Written by leading researchers in their respective fields, those articles are commissioned by the Editorial Board.

Formerly known as *Superlattices and Microstructures*, with a 2021 IF of 3.22 and 2021 CiteScore of 5.4

SUPERLATTICES AND MICROSTRUCTURES

Journal Impact Factor ™

2021	Five Year
3.22	**2.434**

JCR Category	Category Rank	Category Quartile
PHYSICS, CONDENSED MATTER *in SCIE edition*	34/69	Q2

Source: Journal Citation Reports 2021. Learn more

Journal Citation Indicator ™ New

2021	2020
0.48	**0.47**

JCI Category	Category Rank	Category Quartile
PHYSICS, CONDENSED MATTER *in SCIE edition*	36/79	Q2

The Journal Citation Indicator is a measure of the average Category Normalized Citation Impact (CNCI) of citable items (articles and reviews) published by a journal over a recent three year period. It is used to help you evaluate journals based on other metrics besides the Journal Impact Factor (JIF).

Learn more

168 (2022) 207301

Contents lists available at ScienceDirect

Micro and Nanostructures

journal homepage: www.journals.elsevier.com/micro-and-nanostructures

The influence of TMGa pre-flow time and amount as surfactant on the structural and optical properties of AlN epilayer

Gamze Yolcu [a,b], Irem Simsek [a,b], Reyhan Kekul [a,b], Ismail Altuntas [a,b], Sabit Horoz [a,c], Ilkay Demir [a,b,*]

[a] Nanophotonics Research and Application Center, Sivas Cumhuriyet University, 58140, Sivas, Turkey
[b] Department of Nanotechnology Engineering, Faculty of Engineering Sivas Cumhuriyet University, 58140, Sivas, Turkey
[c] Department of Metallurgical and Materials Engineering, Faculty of Engineering and Natural Sciences, Sivas University of Science and Technology, 58140, Sivas, Turkey

ARTICLE INFO

Keywords:
AlN
Characterization
MOVPE
TMGa pre-flow time/amount

ABSTRACT

AlN is used as a template layer for deep UV (DUV) emitter and detector applications, because of its wide bandgap and high thermal conductivity. In this study, trimethylgallium (TMGa) source is used as surfactant to improve crystal quality and decrease dislocation density (DD) of AlN layers grown on sapphire (Al_2O_3) substrate surfaces by Metal Organic Vapor Phase Epitaxy (MOVPE) system. TMGa pre-flow time and pre-flow amount that TMGa pre-flow to the nucleation stage are the subjects of two distinct optimization studies. The structural and optical properties of grown AlN are examined by a high resolution X-ray diffractometer (HR-XRD), Raman spectroscopy, and UV–Vis–NIR spectrophotometer, respectively. TMGa pre-flow time and TMGa pre-flow amount determined to obtain high crystal quality AlN epilayers are 2 s and 0.446 × 10^{-5} mol/min, respectively. HR-XRD investigation of these growths yields FWHM values of 159/2718 arcsec and 201/1550 arcsec for the ω (002) and ω (102) scans, respectively.

1. Introduction

III-Nitride alloys with a direct, wide, and adjustable bandgap and a high critical breakdown field have received great interest in the fields of UV optoelectronics and high-power electronics such as light-emitting devices, photodetectors, and field-effect transistors [1–4]. Due to its promising properties such as broad bandgap, UV transparency, strong thermal durability, high breakdown voltage and high conductivity, AlN has recently gained a lot of attention for usage as a template layer for DUV transmitter and detector purposes [5–9]. It has been proved that the use of AlN layer instead of GaN or AlGaN NL in the production of GaN or AlGaN based UV LEDs increases the light output power of the LEDs [10]. The crystal quality of the AlN template has a significant impact on the surface morphology, defect density of AlGaN, and the bottom quantum well active layer of DUV devices [11]. Growing AlN with a smooth surface and low threading dislocation density (TDD) is critical for developing DUV device performance [12]. These dislocations can extend to quantum wells and cause non-radiative recombination centers, thus negatively affecting internal quantum efficiency (IQE). It was observed that the IQE increased when the dislocations in the AlN layer were reduced to obtain highly efficient UV LEDs [13]. AlN layers are often grown on heterosubstrates (sapphire (Al_2O_3), SiC, and Si, etc.) because of not being enough large-scale, cost-effective, and low-defect AlN bulk substrates [14–17]. Due to Al_2O_3 visibility in this wavelength range, low price, wide availability, and high

* Corresponding author. Nanophotonics Research and Application Center, Sivas Cumhuriyet University, 58140, Sivas, Turkey.
E-mail address: idemir@cumhuriyet.edu.tr (I. Demir).

https://doi.org/10.1016/j.micrna.2022.207301
Received 21 April 2022; Received in revised form 25 May 2022; Accepted 2 June 2022
Available online 3 June 2022

thermal stability, an AlN layer grown on Al_2O_3 is indeed the procedure of choice for the fabrication of DUV III-nitride systems. Nevertheless, high-quality AlN produced on the Al_2O_3 substrate has a number of drawbacks [18]. The large lattice mismatch of approximately (13.3%) [19] between AlN and Al_2O_3 results in a high DD which limits device performance [20]. Subsequently, the large mismatch of thermal expansion coefficient between AlN and Al_2O_3 (45.4%) [21] causes tensile stress within the compound growth plane at medium temperatures, leading to severe crack formation during cooling.

The introduction of thin nucleation layers (NLs) at low temperature on Al_2O_3 substrates are a large innovation to overcome this issue [22,23]. The traditional epitaxy of AlN by MOVPE technique often suffers from intrinsic problems such as restricted surface migration of Al adatoms and the extreme gas-phase reactions between trimethylaluminum (TMAl) and ammonia (NH_3) [24–26]. Until today, many methods have been used to improve the quality of epitaxial AlN, such as high-temperature growth, pulsed growth of AlN, migration-enhanced epitaxy, nitridation of the substrate, alternating V/III ratio, and flow-modulation MOVPE [7,25,27–32].

The surfactant method has recently received attention to create high-quality AlN layers. As a result, several surfactants such as silicon and indium have been investigated [33]. Among the surfactants has been also used gallium, which could strongly minimize the DD and improve the surface morphology of AlN layers grown on SiC [34,35]. The utilization of the gallium effect along the initial growth phase on the crystal quality of AlN and GaN layers on the Al_2O_3 substrate has been occasionally studied, until now [36]. The nucleation or buffer layer, which is known to play a critical role in the formation of AlN epilayers [37], is usually the first step of high crystalline quality AlN growth. According to published research, TMGa pre-flow minimizes the possibility of amorphous formations and dislocations between Al_2O_3 and AlN, while also improving the structure's optical quality. Furthermore, it was discovered that adding TMGa flow to the nucleation stage increased nucleation size and reduced stress [36,38]. These results show up that the surfactant effect of TMGa flow gives rise to the nucleation islands becoming bigger, reducing the Al diffusion barrier and increasing the lateral development of AlN, eventuated grain size, and crystal quality, similarly to the indium surfactant effect on GaN growth [38,39].

The structural quality and surface morphology of the created later AlN layers have been observed to be significantly dependent on the distribution of AlN nucleation islands, which is significantly affected by the short diffusion length and high sticking coefficient of Al atoms [25]. However, it is not yet fully understood how Ga atoms improve the crystal quality of AlN layers. It is of attention to study the effect of sent TMGa in the coalescence of AlN before the nucleation stage and a decrease in stress.

In this study, we try to understand better the effect of TMGa conditions on high-temperature AlN layers grown on the Al_2O_3 substrate. Also, in order to obtain an improved quality of AlN, we enable the determination of the TMGa pre-flow amount and duration. In this context, optical and structural properties were analyzed to comment on the mechanism leading to improved AlN layer quality. Before starting NL growth, TMGa pre-flow was studied at certain times. Although there were studies examining the effect of TMGa on growth, there was no such pre-flow effect study in the literature. The improved high-quality AlN epilayers would be advantageous to the improvement of the UV optoelectronic and power electronic devices.

2. Experimental part

Six samples of AlN were grown by high-temperature MOVPE on 2-inch c-plane substrates in an Aixtron 200/4 RF-S low pressure, horizontal-flow MOVPE system with radio frequency (RF) heating to investigate the effect of a TMGa pre-flow. TMAl, TMGa, and NH_3 were used as precursors for Al, Ga, and N, respectively. The mixture of H_2 and N_2 was used as a carrier gas for the then growth and the growth pressure was kept at 50 mbar. Substrates were exposed to in situ H_2 atmosphere at 1380 °C for 10 min before growth begin. In these studies, an optimized AlN NL was formed that grows on the substrate at a surface temperature of 1080 °C and a reactor pressure of 50 mbar. This NL was conventionally grown with simultaneously supplied TMAl (14 sccm) and NH_3 (1200 sccm) and the growth rate was ~0.09 nm/s. Three different flows were made at 0, 3, and 5 s in order to investigate the effect of the appropriate time of TMGa pre-flow on the properties of the AlN layers grown on substrate. During the growth, the flow rate of TMGa was kept constant at 3.88×10^{-5} mol/min. The appropriate TMGa pre-flow time was decided as 2 s with this study. Then, three different flow studies of 3.88×10^{-5},1.78×10^{-5}, and 0.446×10^{-5} mol/min, respectively, were conducted to investigate the effect of the appropriate amount of TMGa pre-flow. Then AlN layer structures were grown by using the pulsed atomic-layer epitaxy (PALE) technique with optimized changing of TMAl pulses (4-s) and NH3 pulses (2-s). TMAl and NH_3 flow for this layer were 77 sccm and 900 sccm, respectively while the reactor pressure was 50 mbar during the growth. Table 1 provides information on the growth parameters of the samples examined. The crystalline quality analysis of these AlN layers was performed using 4 bounce Ge (220) monochromator HR-XRD. The Raman spectroscopy was recorded at room temperature (WITech alpha 300 R). Transmittance spectra of the deposited AlN layers grown on substrates were recorded by a double-beam UV–Vis–NIR spectrophotometer (Cary 5000, Varian).

Table 1
Growth parameters of samples.

Samples	TMAl (sccm)	NH_3 (sccm)	TMGa Flow (mol/min)	TMGa Pre-flow Time (s)	Growth temperature (°C)
A	14	1200	3.88×10^{-5}	0	1080
B	14	1200	3.88×10^{-5}	2	1080
C	14	1200	3.88×10^{-5}	5	1080
D	14	1200	0.446×10^{-5}	2	1080
E	14	1200	1.78×10^{-5}	2	1080
F	14	1200	3.88×10^{-5}	2	1080

3. Results and discussion

To increase the crystal quality of the structure, systematic growth mechanisms and characterization investigations of the AlN layers with TMGa pre-flow were carried out. In this context, firstly the effect of TMGa pre-flow time on the quality of AlN film was investigated.

The surface condition was controlled during the growth of AlN films by in-situ optical reflectance measurements as given in Fig. 1. Colored lines at the left bottom of the Fig. 1 show the flow state of the source gases for Sample B during growth. Before the NL formation of AlN, 2 s of simultaneous flow of TMGa, TMAl, and NH_3 gases can be visible. During the growth, TMAl (4 s) and NH_3 (2 s) gases using PALE techniques were flowed, respectively. As there are 5 s of simultaneous flow of TMGa for Sample C and no TMGa pre-flow for Sample A, they are not shown in the flow diagram. It can be seen that the AlN film growths include pulsed flows. Samples A, B, and C have nearly the same epitaxial reflectivity curve, revealing that there is no clear effect on surface situation of AlN epilayers.

HR-XRD rocking curve measurements were made to understand the structural properties of the grown samples. Peak positions and their broadening observed in the ω-2θ scans measured with HR-XRD may show the relaxation and crystalline quality of samples. Fig. 2 shows a 2θ-ω scan with three peaks around 34.7°, 36.0°, and 37.8°, as well as a substrate peak at 41.66°. When the flow time of the TMGa gas is increased, that is, the ratio of Ga sent to the surface increases, it is seen that the intensity of the peaks around 34.7° and 37.8° increases. The most evident peak at 34.7°and 37.8° are seen when there is the 5 s TMGa pre-flow. The peak around 36.0° belongs to AlN(002) while the peak around 34.7° belongs to GaN(002) growing at the interface due to TMGa pre-flow. Although it is noticed that the peak around 37.8° increases as the TMGa flow time increases, it is not determined which layer causes this peak. Our investigation into this matter is still ongoing.

It is seen that the FWHM value of the sample grown without TMGa pre-flow is higher compared to the others when the inset graph in the Fig. 2 is examined. It was observed that the FWHM value decreased when 2s TMGa flow was applied, and the FWHM value increased with increasing TMGa pre-flow to 5 s. It was observed that when the TMGa pre-flow was increased from 2 s to 5 s, both screw and edge type dislocation density (ETDD) increased. According to research published in the literature, FWHM values decreased as the TMGa pulse time grew, and FWHM values increased somewhat as the TMGa pulse period more increased [25]. Our study backs us up on this.

TMGA flow affects DD, as illustrated in the HR-XRD scans below. Fig. 3a indicates the graphics of the symmetric (002) ω-scan AlN layer associated with screw-type dislocation density (STDD), and Fig. 3b reveals the graphics of the asymmetric (102) ω-scan associated with mixed-edge type dislocation density. The STDD is high and the ETDD is low when grown without TMGa pre-flow. The high STDD has been attributed to the formation of many small islands when grown without TMGa pre-flow. Dislocations and surface pits are formed by the coalescence of these small islands [34]. When 2s TMGa flow was applied, the STDD decreased and the ETDD increased slightly. TMGa pre-flow is thought to make the nucleation islands expand, lowering the STDD. Increasing the TMGa flow too much causes larger nucleation sites and consequently the formation of larger islands of nucleation and larger dislocations [25]. Therefore both screw and edge type dislocation density increased when the TMGa pre-flow was increased from 2s to 5s. The predominant dislocation in the film is the edge dislocation generated by the substantial mismatch between the AlN epilayer and the substrate, as seen in the samples in this research. ω (002) and ω (102) FWHM values of Samples A, B and C are 226/2578, 159/2718 and 233/3068 arcsec, respectively. When the FWHM values in ω (002) and ω (102) scans are compared, it can be seen Sample B with the lowest ω (002) FWHM and Sample A with the lowest the ω (102) FWHM. However, Sample B should be preferred because of ~30% decrease in ω (002) FWHM and ~9% increase in ω (102) FWHM compared to Sample A. The 2θ-ω scan FWHM values in Fig. 2 also support this result. Measurements demonstrate that TMGa pre-flow is an important growth parameter that affects crystal quality.

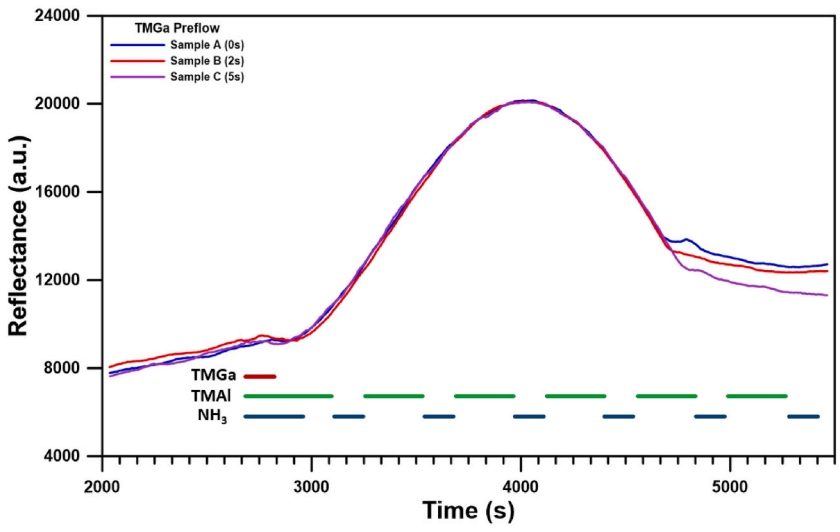

Fig. 1. The in situ reflectance recorded during the growth process for Samples A, B, and C.

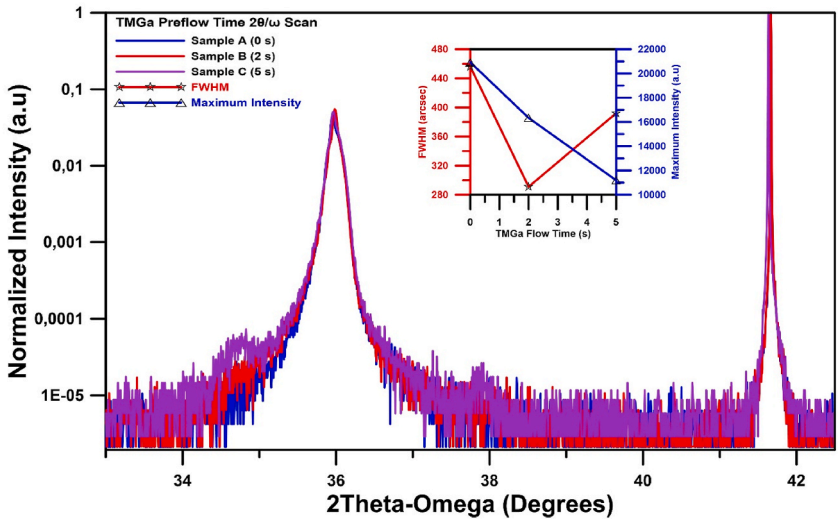

Fig. 2. Effect of TMGa pre-flow time on HR-XRD 2θ-ω scan.

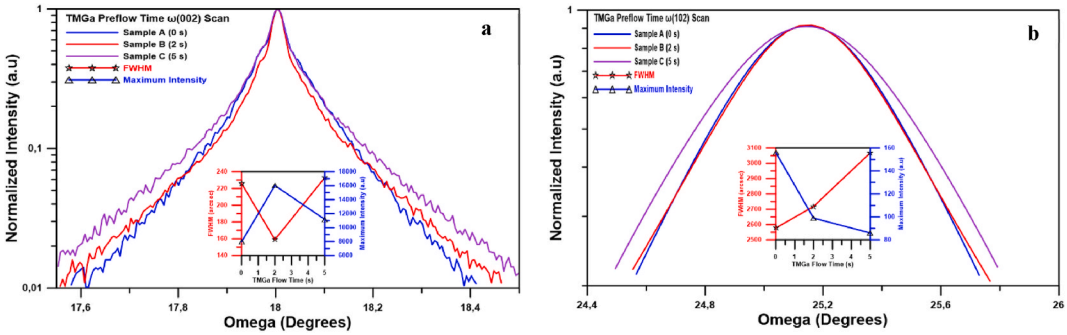

Fig. 3. Effect of TMGa pre-flow time on HR-XRD a ω (002) scan and b ω (102) scan.

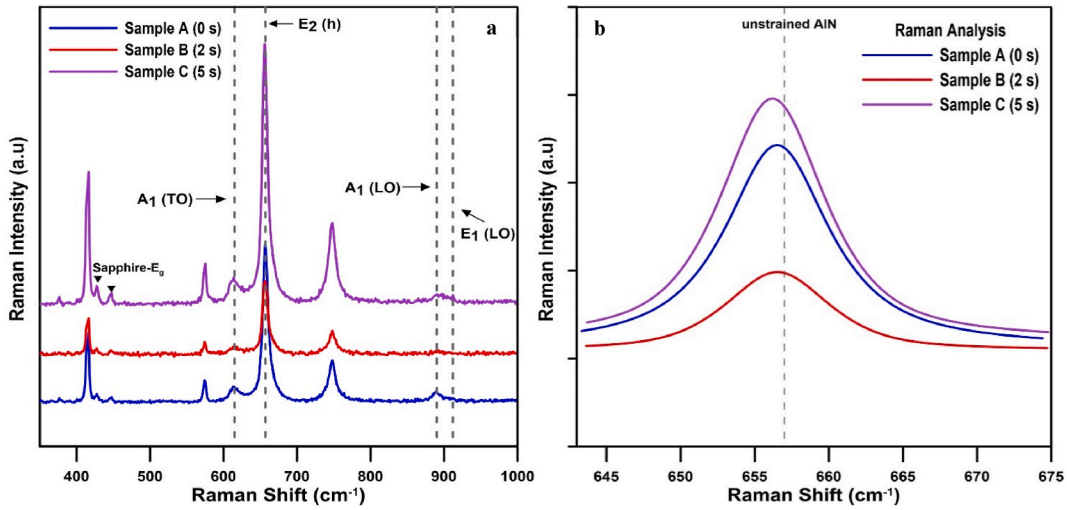

Fig. 4. a Raman spectra from 350 cm^{-1} to 1000 cm^{-1} for PALE AlN films with various TMGa pre-flow time deposited on substrate and **b** Gaussian fit graph of the AlN-E2.

Raman spectra for the first three samples in the current study are displayed in Fig. 4a. Also, Fig. 4b shows Gaussian fits of the E_2 (high) mode of these samples. In Raman analysis, a good quality c-oriented AlN wurtzite structure determines only within non-polar E_2 (high) and A_1 (LO) phonons modes. In addition, it is known that the forbidden mode in c-oriented wurtzite AlN is generally appering around 615 cm^{-1} [25,40]. E_2 high peak seen at a lower frequency than the unstrained AIN-E_2 high phonon mode show residual tensile stress, while E_2 high peaks seen at higher frequencies show residual compressive stress [41]. The mode is only affected by strain [39]. Therefore, it is a good sign for strain fields. The E_2 high phonon mode which provides knowledge about in-plane strain marked by the dashed line specifies the unstrained AlN frequency at 657.4 cm^{-1} [42]. The peak locations of the E_2 high mode in our Samples (A, B, and C) are determined to be approximately 656.50 cm^{-1}. Also as shown in Fig. 4a, specific A_1(TO) forbidden phonon modes has observed in all samples. The problem might be caused by crystallites (facets) being disoriented in relation to the sample surface [43]. In our situation, Sample B has a lower intensity of the A_1 (TO) forbidden phonon mode than the others. It means that Sample B exhibits a superior single crystallographic orientation along the c-axis than the others, indicating that it helped to create c-oriented AlN layers.

Defects influence strongly impact the optical properties of AlN-based optoelectronic devices [44]. The variation of the transmittance of the samples belonging to the TMGa pre-flow time study according to the wavelength is shown in Fig. 5. The spectra reveal a crisp interface between AlN thin films and substrate, as seen by the well-defined interference patterns. The number of interference fringes is equal for Sample A, B, and C. This observation indicates samples have approximately the same thickness [45]. Moreover, there are many studies in the literature show that the transmittance level decrease when surface roughness of thin film increases [46–48]. Wiatrowski et al. stated that the transmittance value decreased when the roughness was high enough [47]. Larena et al. showed schematically that surface roughness caused high light scattering and increased absorption. The main reason for the decrease in transmittance value is high light scattering because the increase in absorption is negligible [46]. In our study, we have observed that the optical transmittance decreases as the TMGa pre-flow time increases. The drop in transmittance values is considered to be related to the influence of increased TMGa pre-flow time due to increased roughness of the film surfaces. Sample C has the lowest transmittance of the three samples, suggesting the presence of the most flaws, as shown by HR-XRD. Comparing the transmittance measurements of Sample A and Sample B suggests that the surface roughness of Sample A is slightly lower than that of Sample B. The effective optical band gap Eg of the layer can be estimated by taking the linear portion from a plot of $(\alpha h\nu)^2$ versus photon energy ($h\nu$), as shown in Fig. 6. In Sample C, Eg decreases from 6.12 to 6.10 eV. These values are slightly lower than the values reported for bulk AlNin the literature which is attributed to the variation of strain along these axes [49]. Generally, the increase of absorption band energy is attributed to the improved crystal quality with TMGa pre-flow.

Based on these measurements, it is seen that the TMGa pre-flow time affects the crystal quality. When these results were obtained from HR-XRD, UV–Vis–NIR spectrophotometer, and Raman spectroscopy analysis are taken into account in the growths made by changing the TMGa pre-flow times, 2s flow time (Sample B) has chosen for the next optimization study that is of TMGa flow amount. Then, it is desired to investigate the effect of TMGa pre-flow amount on the crystal quality during the selected pre-flow time. To observe the amount effect, three samples are grown 0.446×10^{-5}, 1.78×10^{-5}, and $3.88xx10^{-5}$ mol/min respectively.

Fig. 7 shows the in-situ epitaxial reflectivity curve with monitoring during the growth of Samples D, E and F. Colored lines at the left bottom of the figure indicate the flow state of the source gases during growth as in Fig. 1 (TMGa, TMAl, and NH_3 from top to bottom, respectively).

The general behavior of the film surfaces at growth under different TMGa pre-flow, the amplitude of the reflection curves is quite similar to each other, as can be seen in Fig. 7, which proves that there is no deterioration of the surface during growth. This demonstrates that the amount of TMGa pre-flow does not affect the surface properties excessively.

Fig. 8, Fig. 9a and Fig. 9b reveal the 2θ-ω, ω (002) and ω (102) scans of the second set samples, respectively. In the 2θ-ω scan as

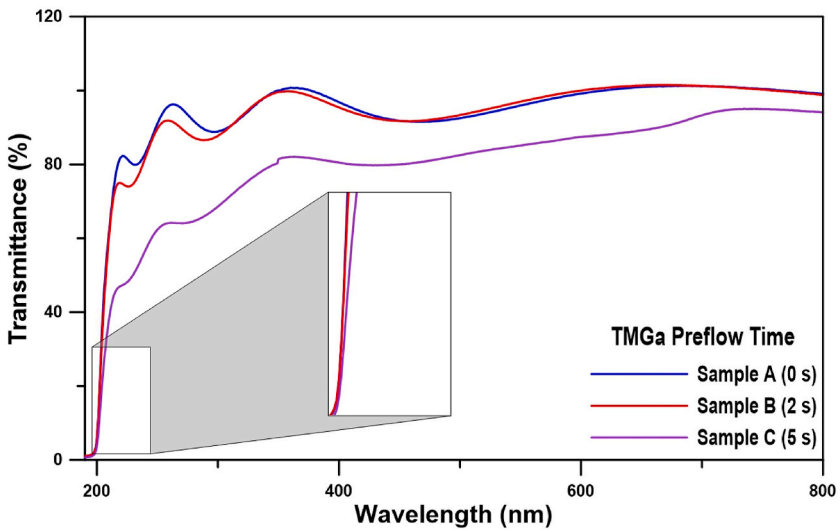

Fig. 5. Transmittance versus wavelength of the samples belonging to the TMGa pre-flow time.

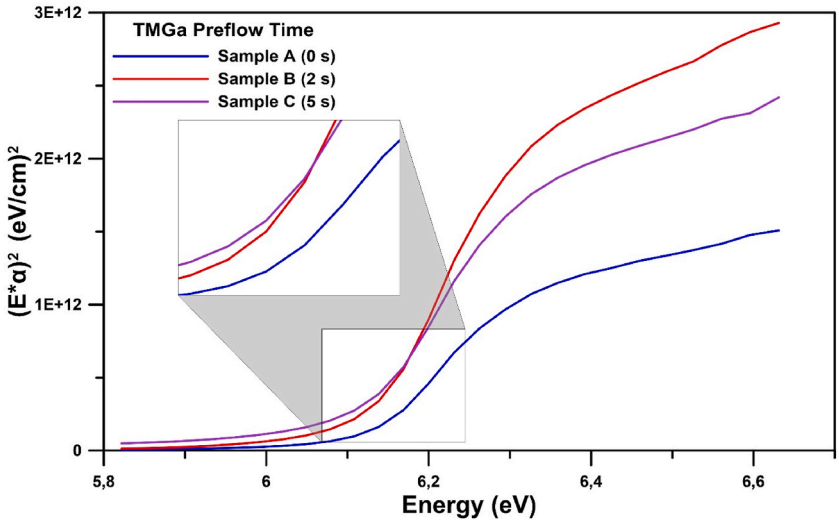

Fig. 6. $(E^*\alpha)^2$ versus the energy of the samples belonging to the TMGa pre-flow time.

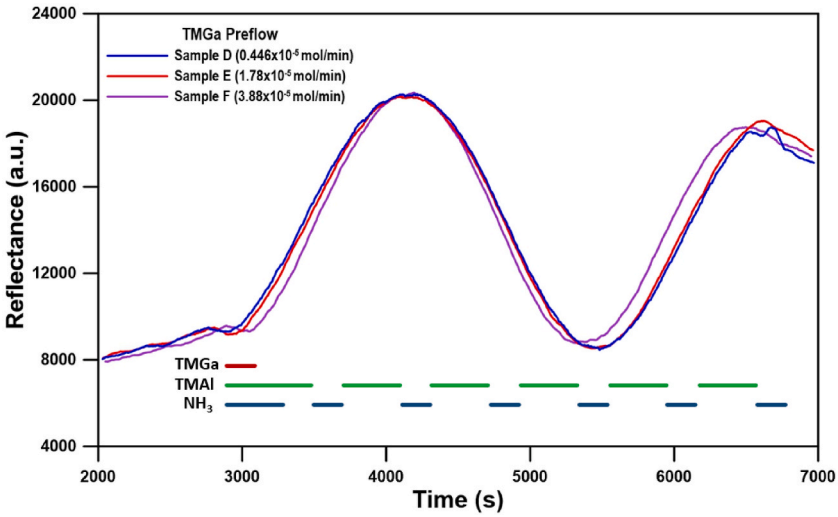

Fig. 7. The in situ reflectance recorded during the growth process for Samples D, E, and F.

similar to the first set, one sees produced from high-intensity sharp peaks on the substrate around 41.66°, as well as AlN peaks about 36.0°. Also, the unexpected peak noticed in the first set's HR-XRD findings is present in this set, and it can be seen that it is placed at 37.8°. We can observe this peak in the 2θ-ω scan of Sample F, but the strength of the peak has diminished to nearly non-existent in Sample E, and there are no unexpected peaks in Sample D. It is noticed that the unexpected peak disappears with the decrease of TMGa flow, and the FWHM value also decreases when these three samples are examined. The FWHM values obtained from ω (002) scan and ω (102) scan for Samples D, E, and F are 201/1550, 203/1590, and 290/1372 arcsec, respectively. The FWHM values of the ω (002) and ω (102) scans have changed significantly with the amount of TMGa pre-flow. As mentioned above, FWHM values prove that low-density screw dislocation occurs and the main dislocation in the film is the edge dislocation caused by the large mismatch between the AlN epilayer and the substrate. The highest crystal quality is found at the stage when the TMGa pre-flow quantity is 0.446×10^{-5} mol/min, according to the FWHM values of the ω (002) and ω (102) scans.

The recorded Raman spectra for Samples D, E, and F and Gaussian fit plots are indicated in Fig. 10a and Fig. 10b, respectively. As can be seen in Fig. 10b, the peak positions of the E2 high mode for Samples D, E, and F have been found as 656.50, 655.35, and 655.35 cm−1, respectively. Samples E and F have the same peak value and are on the lower frequency side of the unstrained position, which determines the residual tensile stress. It means that Sample D has less residual tensile stress and a better single crystallographic orientation along the c-axis than the other samples. Residual stress can have two basis, the first being a compensatory effect of lattice expansion due to TMGa flux and the second being related to the intrinsic stress occurred from a change in growth mode and coalescence of nucleation islands by TMGa flux causing [25,36]. Indeed, a certain time and amount TMGa pre-flow before the growth lead

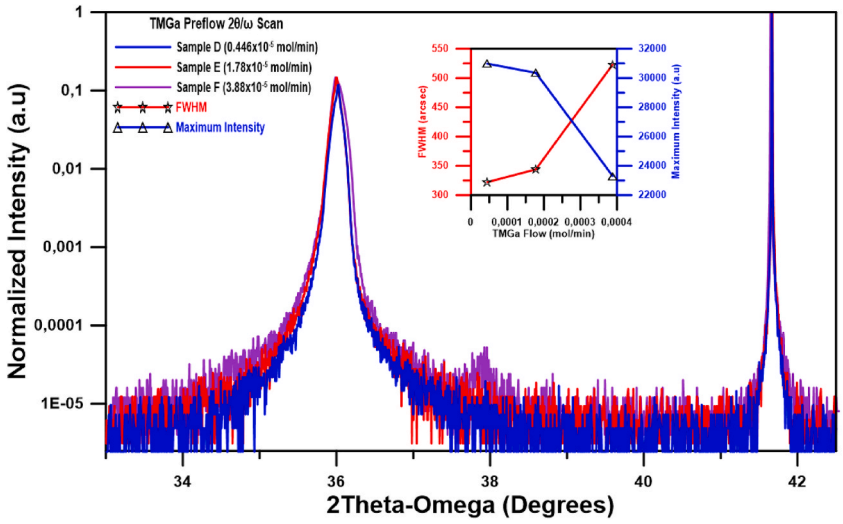

Fig. 8. Effect of TMGa pre-flow amount on HR-XRD 2θ-ω scan.

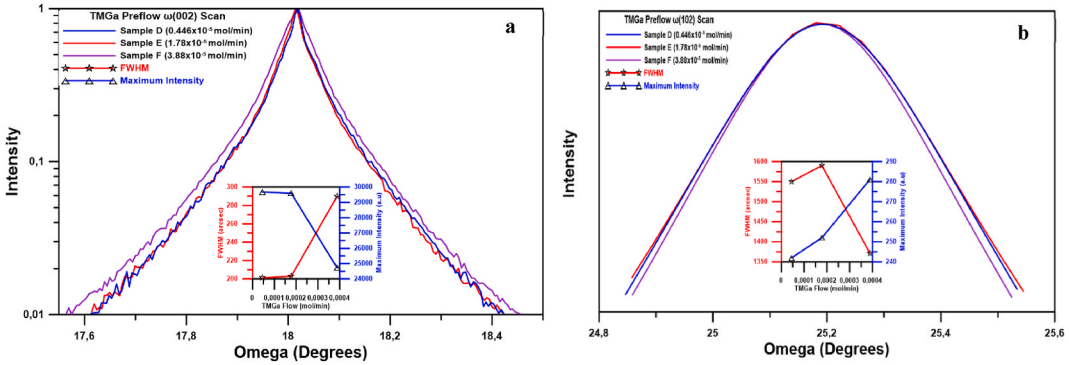

Fig. 9. Effect of TMGa pre-flow amount on HR-XRD **a** ω (002) scan and **b** ω (102) scan.

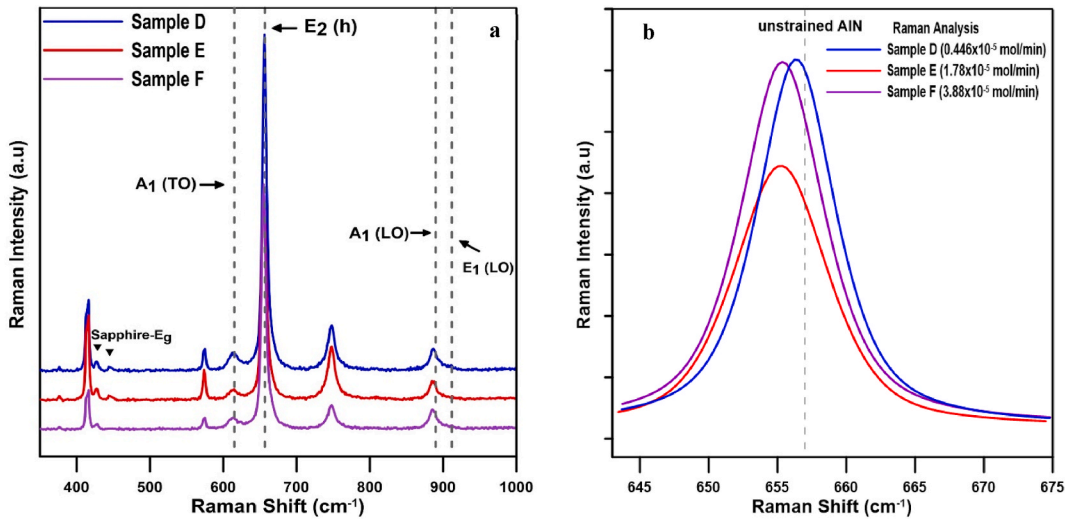

Fig. 10. a Raman spectra from 350 cm^{-1} to 1000 cm^{-1} for PALE AlN films with various TMGa pre-flow amounts deposited on substrate and **b** Gaussian fit graph of the AlN-E2.

to an improved optical quality accompanied by decreased residual tensile strain. It has been proven by Raman and spectroscopy measurements for current samples.

The in-plane compressive stress can be calculated using equation (1):

$$\sigma = \frac{\lambda_R - \lambda_o}{K} \tag{1}$$

where K (4.3 cm^{-1} GPa^{-1}) is the pressure coefficient, and $\lambda_R - \lambda_o$ is the phonon peak shift [50], while the in-plane compressive strain can be calculated by equation (2):

$$\varepsilon = \frac{\sigma}{\Upsilon} \tag{2}$$

where ϒ (469 GPa) is the biaxial stress of AlN, and σ is the in-plane compressive stress [51].

On the other hand, the crystal quality of the AlN epilayer can be defined by the FWHM value of the E_2 (high) mode because extended defects lead to a broadening of this mode [50]. The FWHM of the E_2 (high) mode is 7.23 cm^{-1}, 8.12 cm^{-1}, and 6.83 cm^{-1} for the Samples D, E, and F, respectively. Sample D has the lowest FWHM value, as seen in Fig. 11. These findings show that the increased crystal quality of the AlN epilayer agrees well with HR-XRD results. The stress and strain calculations given above were made for both sets and given in the Fig. 11.

After that, optical transmission measurements in the wavelength range of 200–800 nm are performed on the substrate. All the films exhibit high transmittance in the visible and near IR regions, especially there are samples that have a transmittance higher than 90%, as shown in Fig. 12. The material is nearly transparent above the 210 nm wavelength region. However, it is observed that the highest transmittance is Sample D and the lowest transmittance is Sample F. As a consequence, this result implies that Sample D's crystal quality is superior to Sample F's. As shown in Fig. 13, the bandgaps of Samples D, E, and F are calculated to be around 6.16 eV, with the predicted bandgap of AlN being somewhat less than the stated value for AlN [17].

4. Conclusions

In the present study, the TMGa preflow method applied to grow a high crystal quality AlN epilayer on substrate using the MOVPE system was reported. HR-XRD, UV–Vis–NIR spectrophotometer, and Raman spectroscopy were used to assess the suggested growth method's influence on the structural and optical characteristics of current samples. TMGa pre-flow time and amount were the subjects of two optimization experiments for this investigation. As a result of the characterization studies, the optimum values of TMGa pre-flow time and amount were determined as 2 s and 0.446×10^{-5} mol/min, respectively. An improvement in the structural and optical properties of the films was observed when the optimum amount of TMGa pre-flow. As both the pre-flow time and the amount of pre-flow increased (the ratio of TMGa increased in the medium), unexpected peaks were observed in both HR-XRD scans, and it was noticed that the optical quality of the films deteriorated according to the situation as a result of UV–Vis–NIR spectrophotometer and Raman spectroscopy measurements.

For the first time, the TMGa pre-flow effects have been thoroughly investigated in this study. These findings are promising for the performance of devices to be used AlN epilayer.

Data availability statements

The datasets generated during and/or analyzed during the current study are available from the corresponding author on reasonable request.

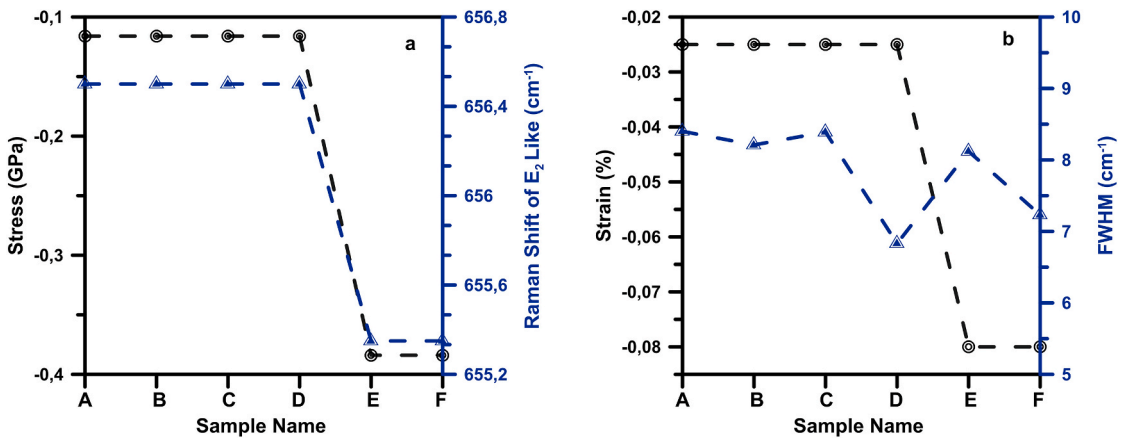

Fig. 11. a The calculated stress and Raman shift of samples **b** the calculated strain and FWHM of samples.

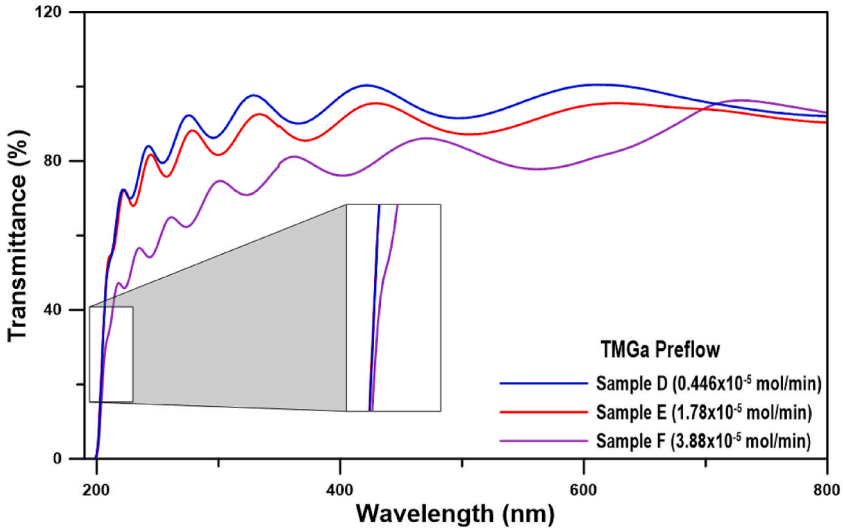

Fig. 12. Transmittance versus wavelength of the samples belonging to the TMGa pre-flow amount.

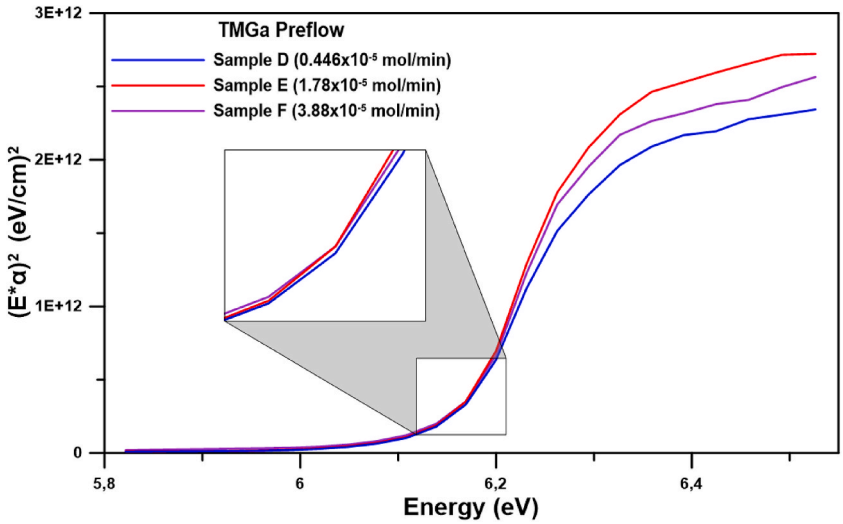

Fig. 13. $(E^*\alpha)^2$ versus the energy of the samples belonging to the TMGa pre-flow amount.

Credit author statement

Gamze Yolcu: Conceptualization, investigation, writing – original draft. Irem Simsek: Investigation, writing – review & editing. Reyhan Kekul: Investigation, writing – review & editing. Sabit Horoz: Investigation, writing – review & editing. Ismail Altuntas: Investigation, formal analysis, funding acquisition. Ilkay Demir: Funding acquisition, Methodology, Project administration, Supervision, Writing – review & editing.

Declaration of competing interest

The authors declare that they have no known competing financial interests or personal relationships that could have appeared to influence the work reported in this paper.

Acknowledgments

The authors acknowledge the usage of the Nanophotonics Research and Application Center at Sivas Cumhuriyet University (CUNAM) facilities. This work is supported by the TÜBITAK, The Scientific and Technological Research Council of Turkey, under project number 118F425.

References

[1] I. Bryan, Z. Bryan, S. Washiyama, P. Reddy, B. Gaddy, B. Sarkar, M.H. Breckenridge, Q. Guo, M. Bobea, J. Tweedie, S. Mita, D. Irving, R. Collazo, Z. Sitar, Appl. Phys. Lett. 112 (2018) 6.
[2] S. Zhao, H.P.T. Nguyen, M.G. Kibria, Z. Mi, Prog. Quant. Electron. 44 (2015) 14–68.
[3] I. Altuntas, M.N. Kocak, G. Yolcu, H.F. Budak, A.E. Kasapoğlu, S. Horoz, E. Gür, I. Demir, Mater. Sci. Semicond. Process. 127 (2021), 105733.
[4] X. Zhao, B. Tang, L. Gong, J. Bai, J. Ping, S. Zhou, Appl. Phys. Lett. 118 (18) (2021), 182102.
[5] B. Tang, Z. Wan, H. Hu, L. Gong, S. Zhou, Appl. Phys. Lett. 118 (26) (2021), 262101.
[6] G.A. Slack, R.A. Tanzilli, R.O. Pohl, J.W. Vandersande, J. Phys. Chem. Solid. 48 (7) (1987) 641–647.
[7] F. Brunner, H. Protzmann, M. Heuken, A. Knauer, M. Weyers, M. Kneissl, Phys. Status Solidi C 5 (6) (2008) 1799–1801.
[8] Q.S. Paduano, D.W. Weyburne, J. Jasinski, Z. Liliental-Weber, J. Cryst. Growth 261 (2–3) (2004) 259–265.
[9] Y. Robin, K. Ding, I. Demir, R. McClintock, S. Elagoz, M. Razeghi, Mater. Sci. Semicond. Process. 90 (2019) 87–91.
[10] H. Hu, S. Zhou, X. Liu, Y. Gao, C. Gui, S. Liu, Sci. Rep. 7 (1) (2017) 1–10.
[11] I. Demir, Y. Koçak, A.E. Kasapoğlu, M. Razeghi, E. Gür, S. Elagoz, Semicond. Sci. Technol. 34 (7) (2019), 075028.
[12] X. Zhang, F.J. Xu, J.M. Wang, C.G. He, L.S. Zhang, J. Huang, J.P. Cheng, Z.X. Qin, X.L. Yang, N. Tang, X.Q. Wang, B. Shen, CrystEngComm 17 (2015) 7496.
[13] H. Hu, B. Tang, H. Wan, H. Sun, S. Zhou, J. Dai, L.J. Guo, Nano Energy 69 (2020), 104427.
[14] L.W. Sang, Z.X. Qin, H. Fang, T. Dai, Z.J. Yang, B. Shen, G.Y. Zhang, X.P. Zhang, J. Xu, D.P. Yu, Appl. Phys. Lett. 93 (12) (2008), 122104.
[15] Z. Chen, S. Newman, D. Brown, R. Chung, S. Keller, U.K. Mishra, S.P. Denbaars, S. Nakamura, Appl. Phys. Lett. 93 (2008), 191906.
[16] L. Huang, Y. Li, W. Wang, X. Li, Y. zheng, H. Wang, Z. Zhang, G. Li, Appl. Surf. Sci. 435 (2018) 163–169.
[17] K.M. Pürlü, M.N. Koçak, G. Yolcu, İ. Perkitel, İ. Altuntaş, I. Demir, Mater. Sci. Semicond. Process. 142 (2022), 106464.
[18] I. Demir, H. Li, Y. Robin, R. McClintock, S. Elagoz, M. Razeghi, J. Phys. D Appl. Phys. 51 (8) (2018), 085104.
[19] X. Sun D. Li, Y. Chen, H. Song, H. Jiang, Z. Li, G. Miao, Z. Zhang, CrystEngComm 15 (2013) 6066.
[20] R.G. Banal, Y. Akashi, K. Matsuda, Y. Hayashi, M. Funato, Y. Kawakami, Jpn. J. Appl. Phys. 52 (2013), 08JB21.
[21] W. Wei, Y. Peng, J. Wang, M.F. Saleem, W. Wang, L. Li, Y. Wang, W. Sun, J. Nanomater. 11 (2021) 698.
[22] H. Amano, N. Sawaki, I. Akasaki, Y. Toyoda, Appl. Phys. Lett. 48 (1998) 353.
[23] S. Nakamura, Jpn. J. Appl. Phys. 30 (1991) L1705–L1707.
[24] D.G. Zhao, J.J. Zhu, D.S. Jiang, H. Yang, J.W. Liang, X.Y. Li, H.M. Gong, Elsevier, 2006, p. 289.
[25] H. Wu, H. Wang, Y. Chen, L. Zhang, Z. Chen, Z. Wu, G. Wang, H. Jiang, J. Cryst. Growth 490 (2018) 56–60.
[26] I. Perkitel, I. Altuntaş, I. Demir, Gazi Univ. J. Sci. (2021), https://doi.org/10.35378/gujs.822954.
[27] J.S. Yang, H. Sodabanlu, I. Waki, M. Sugiyama, Y. Nakano, Y. Shimogaki, J. Japanese, Appl. Physics, Part 2 Lett. 46 (2007) 36–40.
[28] M. Takeuchi, H. Shimizu, R. Kajitani, K. Kawasaki, T. Kinoshita, K. Takada, H. Murakami, Y. Kumagai, A. Koukitu, T. Koyama, S.F. Chichibu, Y. Aoyagi, J. Cryst. Growth 305 (2007) 360–365.
[29] M. Imura, N. Fujimoto, N. Okada, K. Balakrishnan, M. waya, S. Kamiyama, H. Amano, I. Akasaki, T. Noro, T. Takagi, A. Bandoh, J. Cryst. Growth 300 (2007) 136–140.
[30] N. Okada, N. Kato, S. Sato, T. Sumii, T. Nagai, N. Fujimoto, M. Imura, K. Balakrishnan, M. Iwaya, S. Kamiyama, H. Amano, I. Akasaki, H. Maruyama, T. Takagi, T. Noro, A. Bandoh, J. Cryst. Growth 298 (2007) 349–353.
[31] I. Simsek, G. Yolcu, M.N. Koçak, K. Pürlü, I. Altuntas, I. Demir, J. Mater. Sci. Mater. Electron. 32 (2021) 25507–25515.
[32] I. Demir, Y. Robin, R. McClintock, S. Elagoz, K. Zekentes, M. Razeghi, Phys. Status Solidi 214 (2017), 1600363.
[33] B. Daudin, G. Mula, C. Adelmann, J. Oullier, S. Moehl, Phys. Rev. B 64 (2001), 195406.
[34] K. Jeganathan, M. Shimizu, T. Ide, H. Okumura, Phys. Status Solidi 240 (2003) 326–329.
[35] T.M. Al Tahtamouni, J. Li, J.Y. Lin, H.X. Jiang, J. Phys. D Appl. Phys. 45 (2012), 285103.
[36] R. Kirste, M.R. Wagner, C. Nenstiel, F. Brunner, M. Weyers, A. Hoffmann, Phys. Status Solidi 210 (2013) 285–290.
[37] H. Wu, W. Zhao, C. He, K. Zhang, L. He, Z. Chen, Superlattice. Microst. 125 (2019) 343–347.
[38] X. Qiu, Z. Lv, Y. He, Z. Wu, H. Jiang, Superlattice. Microst. 131 (2019) 59–65.
[39] W.K. Fong, C.F. Zhu, C.C. Surya, B.H.P. Leung, C.C. Cheng, B. Sundarvel, E.Z. Luo, J.B. Xu, I.H. Wilson, Optoelectron. Mat. Devices. 4078 (2000) 44–57.
[40] S. Ahmad, M.A. Raushan, H. Gupta, S. Kattayat, S. Kumar, S. Dalela, P.A. Alvi, M.J. Siddiqui, Opt. Quant. Electron. 51 (2019) 1–23.
[41] M. Kuball, Surf. Interface Anal. 31 (2001) 987–999.
[42] M.N.A. Rahman, A.F. Sulaiman, M.I.M.A. Khudus, K. Allif, N.A. Talik, S.H. Basri, A. Shuhaimi, Jpn. J. Appl. Phys. 58 (2019) SC1037.
[43] S. Xiao, N. Jiang, K. Shojiki, K. Uesugi, H. Miyake, Jpn. J. Appl. Phys. 58 (2019) SC1003.
[44] L. Chen W. Lin, H. Chen, H. Xu, C. Guo, Z. Liu, J. Yan, J. Sun, H. Liu, J. Wu, W. Guo, J. Kang, J. Ye, Cryst. Growth Des. 21 (2021) 2911–2919.
[45] M. Emam-Ismail, M. El-Hagary, E.R. Shaaban, A.M. Al-Hedeib, J. Alloys Compd. 532 (2012) 16–24.
[46] A. Larena, F. Millán, G. Pérez, G. Pinto, Appl. Surf. Sci. 187 (3–4) (2002) 339–346.
[47] A. Wiatrowski, A. Obstarczyk, M. Mazur, D. Kaczmarek, D. Wojcieszak, Coatings 9 (2) (2019) 106.
[48] J. Ben, X. Sun, Y. Jia, K. Jiang, Z. Shi, H. Liu, D. Li, CrystEngComm 20 (32) (2018) 4623–4629.
[49] M. Feneberg, M.F. Romero, M. Röppischer, C. Cobet, N. Esser, B. Neuschl, K. Thonke, M. Bickermann, R. Goldhahn, Phys. Rev. B Condens. Matter 87 (2013), 235209.
[50] J.Z. Li, Z.Z. Chen, Q.Q. Jiao, Y.L. Feng, S. Jiang, Y.F. Chen, T.J. Yu, S.F. Li, G.Y. Zhang, CrystEngComm 17 (2015) 4469–4474.
[51] M. Miyoshi, A. Watanabe, T. Egawa, Semicond. Sci. Technol. 31 (2016), 105016.